Subsurface Water Movement and Downslope Deformation in Model-Slope Tests by Artificial Rainfall

Yasuhiko Okada,[1)] Hiroyuki Miyajima[2)] and Hirotaka Ochiai[3)]
1) Department of Soil and Water Conservation, Incorporated Administrative Agency Forestry and Forest Products Research Institute, 1 Matsunosato, Tsukuba, Ibaraki 305-8687, Japan (okada10@ffpri.affrc.go.jp)
2) Graduate school of Science, Chiba University, 1-33 Yayoicho, Inageku, Chiba 263-8522, Japan (h.miyajima@graduate.chiba-u.jp)
3) Department of Soil and Water Conservation, Incorporated Administrative Agency Forestry and Forest Products Research Institute, 1 Matsunosato, Tsukuba, Ibaraki 305-8687, Japan (ochi@ffpri.affrc.go.jp)

Abstract

The flowslide is reproduced by the quasi-real scale model-slope tests on river sand by artificial rainfall, in which subsurface water movement and downslope deformation are carefully monitored. The rainfall at the intensity of 100 mm/hour on the specimen formed at loose state (9.0-metre long, 1.0-metre wide, 0.5-metre deep) have brought about the failure at 2,931 sec after the onset of sprinkling. Firstly, the pore-fluid has descended gradually leading to the parallel wetting-front to the base, and the sand specimen has been susceptible to the vertical contraction. From 300 sec before the failure, the equi-potential lines started to bend normally to the model-slope base and the pore-fluid has been subject to downslope flow. At the same time, the soil strain in deep layer has considerably started. The most severe creep deformation has been produced in the deep layer among the upper slope portion on steep slope and the failure has been initiated within this section. The excess pore-pressure has not been observed in the source area. Whereas, severe excessive pressure head has been generated due to the collision of the failed upper slope-mass, leading to liquidization. It suggests that the dependence of flowslide generation must be on the dynamic changes in pore-pressure not in the source area but in the compressed lower slope-section.

Keywords: subsurface water movement, downslope deformation, excess pore-pressure, flowslide, model-slope test

Introduction

Landslide disasters have been recorded for several centuries all over the world, which resulted in the untold numbers of casualties and huge economic losses. With the progress of regional development into unstable hillside areas under the pressure of expanding population and urbanization, the responsibility of landslide hazards on socioeconomic aspects has considerably increased. Within the five types of landslides, falls, topples, slides, spreads, and flows (Cruden, 1991, and Cruden and Varnes, 1996), the flow-type is the most dangerous because it generally shows high mobility on non-steep or even gentle slopes that are usually considered safe against landslide disasters. Bishop (1973), Eckersley (1985 and 1990), Hutchinson (1986), Hungr (1995), and Spence and Guymer (1997) used the term, "flowslides," that show the characteristics of long run-out distance in strong association with the existence of pore-pressure. To reveal the initiation mechanism of flowslides, Casagrande (1971), Castro and Poulos (1977), Seed (1979), Poulos (1981), Ishihara (1993), etc., extensively conducted the geotechnical soil tests, and elucidated that the collapse of loose skeletal structure or meta-stable structure (Hutchinson, 1986) suffered the excessive pore-pressure generation and the decrease of shear resistance. On the other hand, the model-slope tests have been conducted. Because of the difficulties in handling and management of the real scale model-slope, most of the studies have been in the use of small-size slope. However, in these cases, the problems of similarity are of ill-effect. By using quasi-real scale model-slope, Fukuzono (1985) proposed that the initiation time of rainfall-induced slope-failure was a function of inverse of shear velocity. Iverson and LaHusen (1989) pointed out that pore-pressures were dynamically fluctuating during the rapid shearing at failure. Okura et al. (2002) showed that the excess pore-pressure generation due to the negative dilatancy lead to the fast shearing. These studies focused on the initiation time and the changes in excess pore pressure during the flowslide motion. In this study, the authors conduct the quasi-real scale model-slope test with artificial rainfall. The attention is placed on the subsurface water movement and the downslope creep-deformation prior to the initiation of failure as well as the generation of excess pore-pressure leading to the flowslide, in which positive and negative pore-pressures in the sand layer and the movement of

pp. 429–436

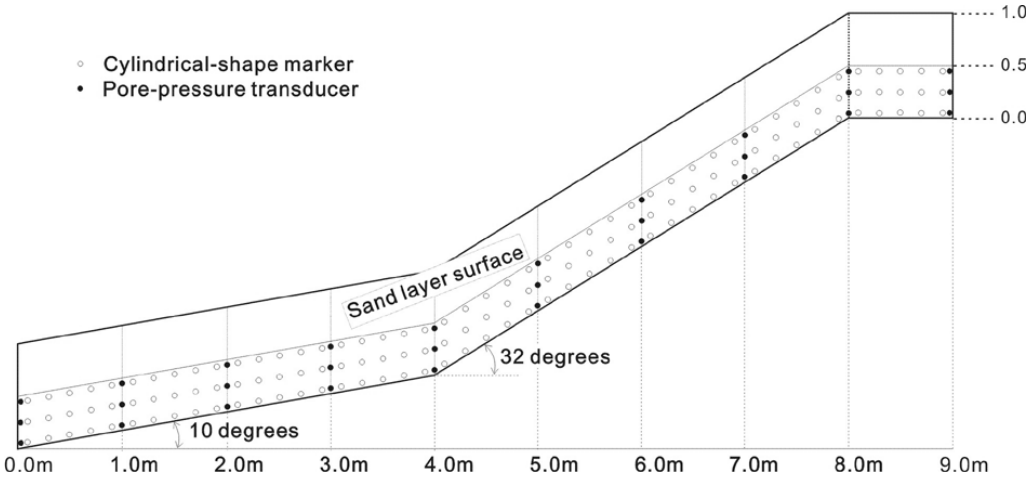

Fig. 1. The side view of the model-flume and arrangement of instruments

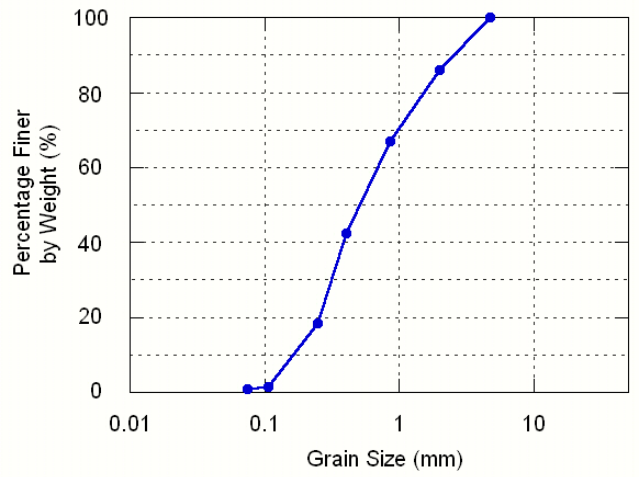

Fig. 2. The grain size distribution curve of the sample

the markers that are embedded in the soil are carefully monitored.

Experimental method

Experimental model-slope and properties of sample

A schematic diagram of the experimental model-slope is shown in Fig. 1. The sand layer surface before the failure and the sizes are shown in the figure. One side of the model-slope is made of the reinforced glass so it is possible to monitor the downslope creep-deformation followed by the flowslide motion. The inclination of the model-slope is in two values. The lower section is set at 10 degrees and the upper is at 32 degrees. The specimen was loosely packed in the model by gently dropping sand from a mobile hopper, where the depth of the layer was at 0.5 m among the whole sections. The artificial rainfall was given by the rain simulator equipped with nozzles at four points all 6.4 metre above the floor along the model-slope. The rainfall intensity was set at 100 mm/hour in the test.

The sand employed was river sand which had been excavated from the Sakuragawa river in Tsukuba city, Ibaraki Prefecture, Japan. The density of sand grains (ρ_s) was 2,620 kg/m^3, the mean diameter (D_{50}) was 0.50 mm, the uniformity coefficient (U_c) was 4.31, the coefficient of curvature (U_c') was 0.93. The grain size distribution curve is shown in Fig. 2.

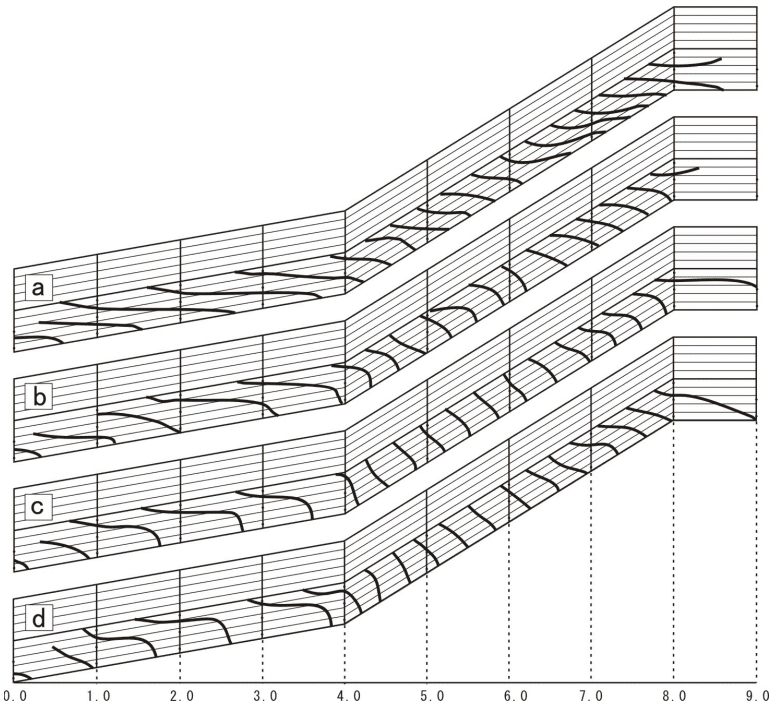

Fig. 3. The changes in equi-potential lines during experiment. The contour interval was set at 0.2 m.

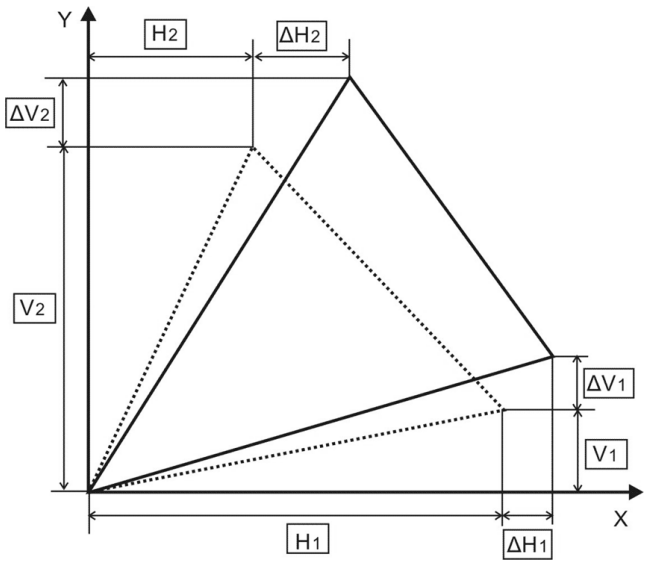

Fig. 4. The deformation of triangle for strain calculation.

Monitoring and data acquisition

The measurement of the positive and negative pore-pressure by pressure transducers and the image analysis of the downslope creep and flowslide motions by tracing the movement of markers embedded in the layer, were carefully conducted. The data acquisition system was developed to simultaneously monitor them such that, the time codes generated by time-code generator were recorded together with pore-pressure measurements, also the time codes displayed in the time-code indicators were filmed by video cameras which were prepared for the image analysis of the specimen deformation.

The changes in pore-pressure were measured by small cylindrical pressure transducers (18 mm in diameter and 83 mm long) that were placed in the sand layer at certain depths indicated in Fig. 1. During the test, the pore pressure transducers moved together with sands until the final deposition after the failure initiation. The soil deformation were filmed by video cameras, in which markers (small cylinders) of 3.0 cm

long and 1.6 cm in diameter buried within the sand were traced. The one bottom side of each marker was adjacent and visible through the reinforced glass. The time-code indicators were placed along the model-slope. The pore-pressure measurements were conducted at 100 Hz, and 30 frames were recorded by video cameras per second.

Results and discussion

Subsurface water movement

The model-slope was failed at 2,931 sec after the commencement of sprinkling of rainfall with 100 mm/hour. The changes in equi-potential line are shown in Fig. 3, in which (a), (b), (c), and (d) are at 900 sec, 300 sec, 60 sec, and 1 sec before the failure initiation, respectively. As Fig. 3(a) shows at 900 sec before the failure, the wetting front roughly travels vertically downward from the sand surface to the base such that each equi-potential line was horizontal and the spaces between arbitrary two equi-potential lines were almost the same in the whole slope section. At 300 sec before the failure (Fig. 3(b)), in the middle part of the model-slope (around 3–6 lengthwise section), the equi-potential lines started to bend normally to the model-slope base, as subsurface water were subject to the downslope directional flow. As the rainfall continued, the euqi-potential lines around 6–8 m lengthwise section also bended normally to the model-slope base, and roughly straight equi-potential lines normal to the model-slope base were found around 4–6 m lengthwise section at 60 second before the failure (Fig. 3(c)). Whereas, the subsurface water conditions around 0–4 m lengthwise section were not changing so much. At 1 second before the failure (Fig. 3(d)), no considerable change in subsurface water conditions from those at 60 second before the failure was observed. However, subsurface water movement in the downslope direction around 4–8 m lengthwise section was conspicuous.

Downslope creep-deformation

Deformation during the experiment was monitored by tracing the markers embedded in the sand. Assuming the plane strain conditions, shear strain ($\gamma_{vh}/2$), horizontal strain (ε_h), and vertical strain (ε_v) were calculated based on the infinitesimal deformation theory as following (Fig. 4):

$$\begin{aligned} \Delta H_t &= \frac{\partial H}{\partial x} \times H_i + \frac{\partial H}{\partial y} \times V_i, \Delta V_i = \frac{\partial V}{\partial x} \times H_i + \frac{\partial V}{\partial y} \times V_i (i = 1, 2) \\ \text{in which } \frac{\gamma_{vh}}{2} &= -\left(\frac{\partial V}{\partial x} + \frac{\partial H}{\partial y} \right), \varepsilon_h = -\frac{\partial H}{\partial x}, \varepsilon_v = \frac{\partial V}{\partial y}. \end{aligned}$$

The obtained values of soil strains around the centre of 2–4, 4–6, and 6–8 m lengthwise section (that is around 3, 5, and 7 m points) at 900, 300, 60, and 1 second before the failure were shown in Fig. 5 in the forms of Mohr' circle. Since the markers were arranged as three rows in the sand layer, the soil strains in deep and shallow sections were calculated. In the figure, the maximum shear strain ($(\gamma/2)_{\max}$) were also marked by open-circles. From the figure, as for the steep model-slope points (7 m (Fig. 5(a) and 5(b)) and 5 m (Fig. 5(c) and 5(d))) and the gentle model-slope section (3 m (Fig. 5(e) and (f))), the Mohr's circles in the deep layer were larger than those in the shallow layer. It signified that the creep-deformation was more progressed in the deep layer and the sands in the shallow layer relatively kept their structure during the experiment. And it should be mentioned that the centre positions of Morh's circle shifted rightward as the test proceeded, indicating the specimen in the whole section was in the contractive deformation. Then, when compared in the deep layers, the circles from the steep model-slope were larger than those from the gentle model-slope. Furthermore, the circles of 7 m deep point were much larger than those of 5 m deep point. Hence, the creep-deformation advanced more on steep slope than gentle slope, and it should be noticed that the upper section on the steep model-slope produced more downslope deformation than lower section on steep slope before the failure initiation.

Fig. 6 shows the inclination of maximum shear strain ($(\gamma/2)_{\max}$) plane from the horizontal axis. As Fig. 6a shows, the inclination of maximum shear strain ($(\gamma/2)_{\max}$) plane of 3-m and 7-m shallow-points kept relatively constant values at around 45 degrees irrespective of the time before the failure. The incident angles (angles between maximum shear strain plane and direction of model-slope base) were at 35 degrees for 3-m point (45–10 degrees) and 13 degrees of 7-m point (45–32 degrees). Whereas the inclination values of maximum shear strain plane from 5-m point were around 32 degrees. Accordingly, the direction of maximum shear strain was corresponded to the model-slope base in the 5-m point. As for the deep-section (Fig. 6b), the inclination was rather constant at around 43 degrees for 3-m point. The inclination for 7-m point increased its values from 34 degrees to 38 degrees, indicative that the direction of maximum shear strain tended to intersect model-slope base more widely as the test proceeded. Whereas, The inclination for 5-m point decreased its values as the test

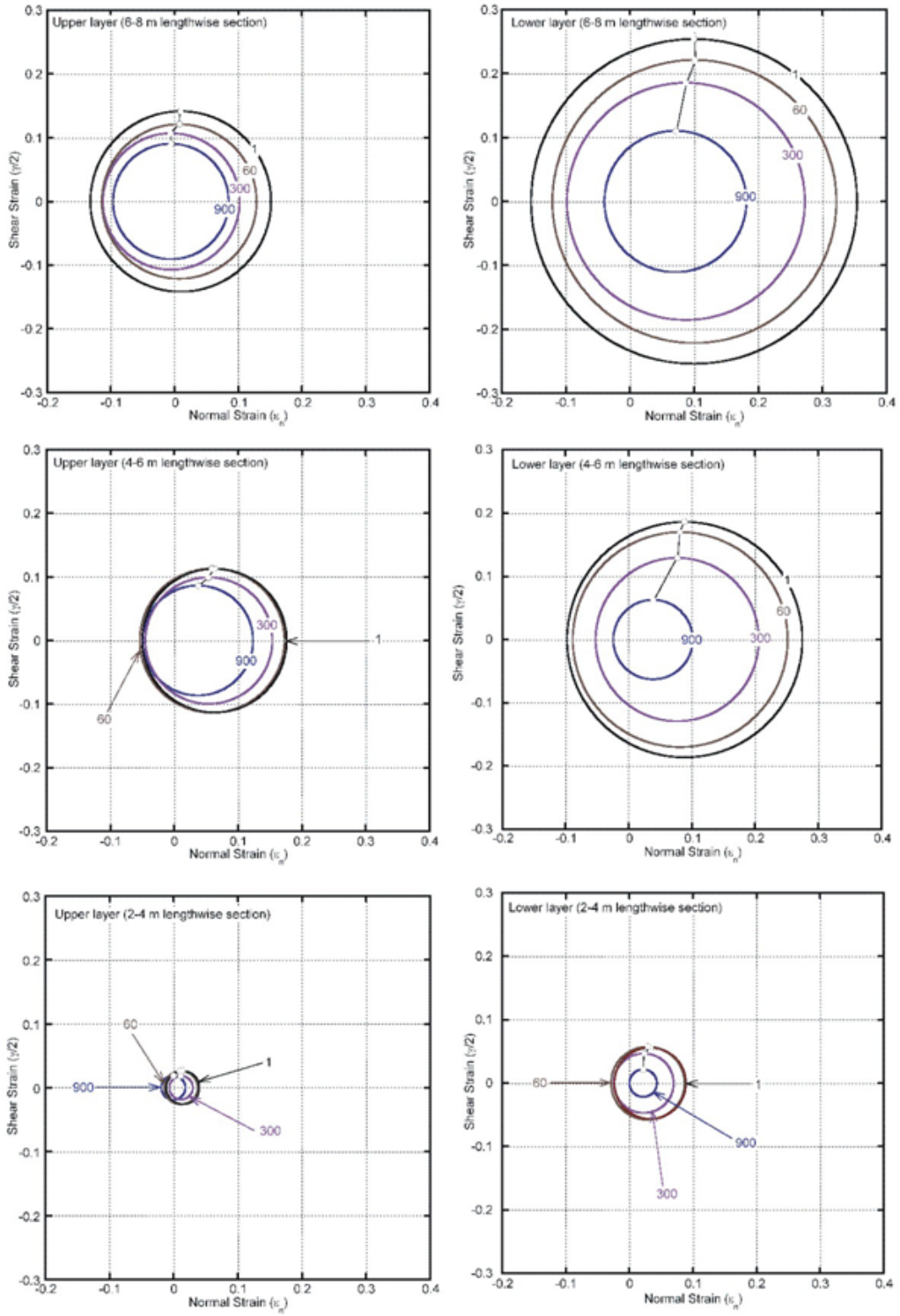

Fig. 5. The changes in strains in the form of Mohr's circles. The shallow layers are shown the left side, and the deep layers are on the right side.

proceeded from 41 degrees to 36 degrees. It meant that the direction of maximum shear strain plane tended to converge to the model-slope base.

As discussed in the previous subsection, the pore-fluid started to flow parallel to the model-slope base around 300 sec before the failure. At around the same time, the soil strains in the deep layer were extended and the Mohr's circles were expanded. It signifies that the formation of water-table inducing the downslope pore-fluid flow associated the deep sand layer with the progress of creep-deformation. Finally, the failure was

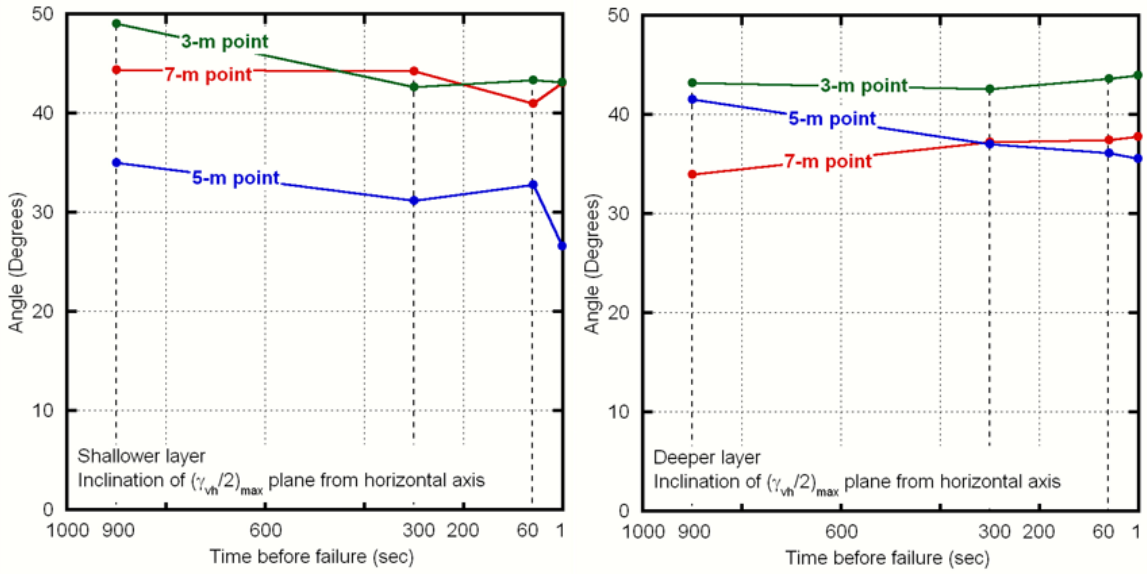

Fig. 6. The changes in inclinations of maximum shear strain plane from the horizontal axis.

initiated around 6–8 m deep-section at 2,931 and the sliding surface was extended to 4–6 m section.

Excess pore-pressure generation

The upper portion along the steep-slope failed firstly, and then the failed mass moved downslope to the lower slope portion. The examination of the pore-pressure generation behaviour in the source area and the compressed zone is conducted. Fig. 7 shows the changes in pore-pressure at 3-m and 7-m lengthwise and 0.45-m deep points. The sand layer thickness on those sensors is also illustrated in the figure. Around 2,931 sec, the sand layer thickness in the source area (7-m point from the lower end) started to decrease, and at the same time, pore-pressure build-up was observed. Once the pore-pressure decreased, however, it reincreased rapidly from 2,933 sec. This is likely because the sliding mass collided against the lower slope section, resulting in the compression to induce the pore-pressure build-up. Since the embedded marker (7-m lengthwise and 0.45-m deep) disappeared during the downslope movement, the sand layer thickness was observed only before 2,932.2 sec. As the pore-pressure did not exceed the sand layer thickness around failure initiation (2,931 - 2,932.2 sec) and the maximum pore-pressure was only 0.36 m, the pore-pressure unlikely exceeded the sand layer thickness during the test, in which excess pore-pressure could have been local and temporary if any. While, the pore-pressure at 3-m point from the lower end suddenly increased at about 2,931.5 sec, it reached as much as 0.78 m (at 2,932.8 sec) roughly within 1 sec. The sand layer thickness increased from 2,932.2 sec to reach 0.60 m at 2,932.8 sec. After that, both of pore-pressure and sand layer thickness gradually decreased, however, the pore-pressure exceeded sand layer thickness from 2,932.2. It means that in the compression zone like 3-m lengthwise point, excess pore-pressure was generated to suffer from liquidization followed by the flowslide motion, in which the undrained sudden loading conditions by failed mass was likely maintained. At 2,932.8 sec the pressure head was 1.3 times as much as the sand layer thickness. Because the excess pore-pressure was generated mainly in the compressed zone of the lower slope-section, it suggests that the dependence of flowslide generation that be associated with the excess pore-pressure within the mass must be on the dynamic changes in the pore-pressure induced not in the source area but in the compressed zone.

Conclusions

From the quasi-real scale model-slope test on loosely packed river sand by artificial rainfall, the followings could be drawn:

1. At the first stage wetting-front traveled vertically down to the model-slope base, in which equi-potential lines were almost horizontal and linear. From 300 sec before the failure, the equi-potential lines started to bend normally to the model-slope base and the pore-fluid was subject to downslope flow. At around the same time, the soil strains in deep layer started considerably to extend;

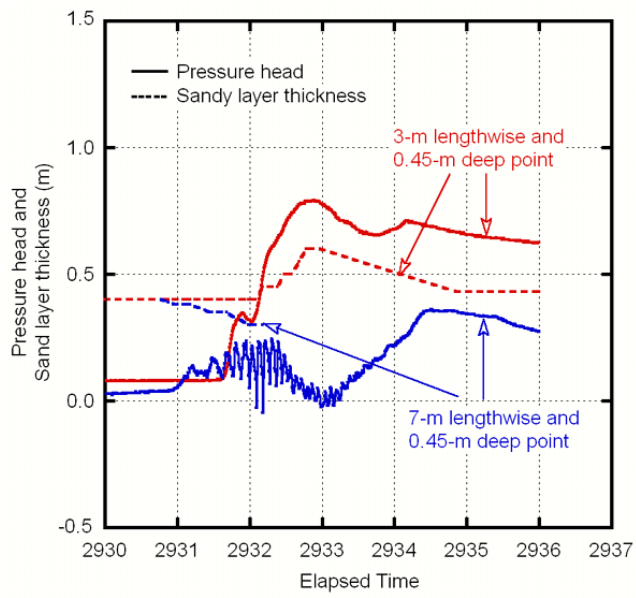

Fig. 7. The relation of pressure head to sand layer thickness

2. The soil strains in shallow layer produced the smaller Mohr's circles than those in the deep layer before the failure. The soil in the shallow layer rather kept their structure, whereas the creep deformation was progressed in the deep layer. Soils in the lower section on gentle slope did not deform largely. The largest Mohr's circles were yielded from the upper slope section on steep slope and the failure was initiated in this section; and

3. In the source area, dynamically changing pore-pressure was observed, but it unlikely exceeded the sand layer thickness. The undrained conditions unlikely maintained and excess pore-pressure was not generated. Whereas, in the compressed zone, the pressure head 1.3 times as much as sand layer thickness was observed. This excess pore-pressure was due to the collision of the upper-slope mass which firstly failed and moved downslope to the lower-slope, it suggested the dependence of flowslide generation was on the dynamic changes in pore-pressure not in the source area but in the compressed lower slope-section.

References

Bishop, A.W. (1973) The stability of tips and spoil heaps. Quarterly Journal of Engineering Geology. **6**, pp. 335–376.

Casagrande, A. (1971) On liquefaction phenomena, report of lecture. Géotechnique. **21**(3), pp. 197–202.

Castro, G., and Poulos, S.J. (1977) Factors affecting liquefaction and cyclic mobility. Journal of Geotechnical Engineering Division, ASCE. **103**(GT6), pp. 501–516

Cruden, D.M. (1991) A simple definition of a landslide. Bulletin of the International Association of Engineering Geology. **43**, pp. 27–29.

Cruden, D.M., and Varnes, D.J. (1996) Landslides types and processed. In special Report 247: Landslides — Investigation and Mitigation. (Turnrer, A.K., and Schuster, R.L., eds.) TRB, National Research Council, Washington, D.C., Chapter 3, pp. 36–75.

Eckersley, J.D. (1985) Flowslides in stockpiled coal. Engineering Geology. **22**, pp. 13–22.

Eckersley, J.D. (1990) Instrumented laboratory flowslides. Géotechnique. **40**(3), pp. 489–502.

Fukuzono, T. (1985) A new method for predicting the failure time of a slope. In Proceedings of 4th International Conference and Field Workshop on Landslides. Tokyo, Japan, 23–31 August 1985. pp. 145–150.

Hungr, O. (1995) A model for the runout analysis of rapid flow slides, debris flows, and avalanches. Canadian Geotechnical Journal. **32**, pp. 610–623.

Hutchinson, J.N. (1986) A sliding-consolidation model for flow slides. Canadian Geotechnical Journal. **23**, pp. 115–126.

Ishihara, K. (1993) Liquefaction and flow failure during earthquakes. Géotechnique. **43**(3), pp. 9–46.

Iverson, R.M., and LaHusen, R.G. (1989) Dynamic pore-pressure fluctuations in rapidly shearing granular materials. Science. **246**, pp. 769–799.

Okura, Y., Kitahara, H., Ochiai, H., Sammori, T., and Kawanami, A. (2002) Landslide fluidization process by flume experiments. Engineering Geology. **66**, pp. 65–78.

Poulos, S.J. (1981) The steady state deformation. Journal of Geotechnical Engineering Division, ASCE. **107**(GT5), pp. 553–562.

Seed, H.B. (1979) Soil liquefaction and cyclic mobility evaluation for level ground during earthquakes. Journal of Geotechnical Engineering Division, ASCE. **105**, pp. 201–255.

Spence, K.J., and Guymer, I. (1997) Small scale laboratory flowslides. Géotechnique. **47**(5), pp. 915–932.